D1.3 – Specification of optoelectronic and plasmonic requirements of single elements

Project Information

Grant Agreement Number	101016706
Project Full Title	photonic system for Adaptable muLtiple-analyte monitoring of fOod-quality
Project Acronym	h-ALO
Funding scheme	RIA
Start date of the project	1st January 2021
Duration	36 months
Project Coordinator	Stefano Toffanin (CNR-ISMN)
Project Website	https://h-alo.eu/

Deliverable Information

Deliverable n°	1.3
Deliverable title	Specification of optoelectronic and plasmonic requirements of single elements
WP no.	1
WP Leader	1-CNR
Contributing Partners	1-CNR, 3-PLAS, 5-WFSR, 8-FhG ENAS
Nature	Report
Authors	Mario Prosa (CNR), Margherita Bolognesi (CNR)
Contributors	Andreas Morschhauser (FhG ENAS) Franco Marabelli (PLASM), Paola Pellacani (PLASM), Eliana Manobianco (PLASM)
Reviewers	Stefano Toffanin (CNR), Mario Prosa (CNR), Margherita Bolognesi (CNR)
Contractual Deadline	M5 (31/05/2021)
Delivery date to EC	14/06/2021

PHOTONICS21

PHOTONICS PUBLIC PRIVATE PARTNERSHIP

Dissemination Level

PU	Public	x
PP	Restricted to other programme participants (incl. Commission Services)	
RE	Restricted to a group specified by the consortium (incl. Commission Services)	
CO	Confidential, only for the members of the consortium (incl. Commission Services)	

Document Log

Version	Date	Description of Change
V1.0	17/05/2021	First draft
V2.0	03/06/2021	Advanced draft with all contributions from partners
V3.0	09/06/2021	Final version including revisions from the coordinator

Table of Contents

1   Executive Summary

The aim of deliverable 1.3 (D1.3) is the identification of the optical characteristics of the optoplasmonic chip components to enable their effective cooperation in a single, miniaturized and integrated chip for localized surface plasmon resonance (LSPR) and plasmon enhanced fluorescence (PEF) detection.

Specifically, the optoplasmonic chip of the h-ALO sensor includes two light-emitting devices, a optically selective photodetector and a nanostructured grating, which is the connection point to the biodiagnostic detection of the analytes of interest. This deliverable is indeed the reference document for the development of the single components that are the objectives of task 2.1, task 2.2 and task 2.3.

In strict correlation with deliverable 1.2 (D1.2) "Specification of analytes and creation of a database of bio-recognition assays and fluorescent labels according to End-user needs", the following document discusses the strategies to ensure the spectral compatibility of the chip components for a dual modality of detection, *i.e.* LSPR and PEF. As a result, the selection of the materials that fulfill the required optical characteristics is introduced.

In details, chapter 2 describes the optical requirements of the single components on the basis of the operation expected by the optoplasmonic chip. For each component, the choice of the composing materials is discussed according to the optical requirements of the whole chip. Chapter 3 focuses on the calculation of the best spectral matching of the subcomponents for the PEF detection, based on the choice of the fluorophores listed in D1.2. Accordingly, chapter 4 introduces the requirements on the optical filter that is likely to be coupled to the photodetector to maximize the signal of PEF detection.

It is worth noting that no specific discussion is reported on the geometrical and operational properties of the chip subcomponents since an in-depth analysis will be included in deliverable 1.4 (due date M20) and deliverable 1.5 (due date M24).

2   Optical requirements of the single organic/hybrid elements

The optoplasmonic chip uses the interaction of 3 different optoelectronic and plasmonic elements, based on organic/hybrid materials, to provide multimodal LSPR and PEF detection. In details, two organic light-emitting diodes (OLEDs), an optically selective organic phototransistor (OPT) and a nanoplasmonic grating (NPG) are the constituting elements of the optoplasmonic chip. For the sake of simplicity, the module including the optically selective OPT and the two OLEDs is hereafter named as photonic module.
Figure 1 shows the design of the chip, in which two detection modalities of LSPR and PEF are independently and simultaneously enabled by the optical excitation of the NPG, operating in a reflection mode. Both optical signals of LSPR and PEF are eventually collected by a single OPT, which converts them into an electrical output signal.

While LSPR is an intrinsic response of the NPG to a change of the refractive index of medium on top of the surface, the PEF detection is activated by means of a fluorophore bound to the surface of the NPG. Considering that PEF and LSPR detection exploit the same optically selective OPT, and that backscattered or reflected light of the excitation source should be not detected in the PEF mode, it follows those two different spectral regions (different OLED emissions) are used to individually excite the LSPR and the PEF detection independently. The two detection modes are simultaneously performed in the same run of detection. However, a sequential activation of the LSPR and the PEF modalities is required because of the use of a single OPT.

In the case of the LSPR detection, the light emitted by the OLED impinges at the NPG and, depending on the analyte on the NPG surface, it is modulated in terms of intensity and then reflected-back to the OPT. The light emitted by the OLED for LSPR should therefore match i) the maximum of the spectral sensitivity of the NPG for LSPR detection and ii) the spectral response of the OPT.

Concerning the PEF detection, the light emitted by the other OLED excites the fluorophores, which are in proximity of the NPG surface. The fluorophore emission is eventually detected by the OPT. In the PEF detection, the photophysical properties of the fluorophore are enhanced by the interaction with the plasmonic properties of the NPG. As a result, a strong compatibility needs to be ensured between i) the spectrum of emission of the OLED for PEF, ii) the transmittance spectrum and the plasmonic modes of the NPG, iii) the spectral absorption and emission of the fluorophore, and iv) the spectral response of the OPT. To improve the

fluorescence signal-to-noise ratio and to avoid the absorption of the backscattered excitation light by the OPT, an optical filter is integrated onto the OPT to produce the optically selective OPT.

It is important to remark that the LSPR characteristics of the NPG are strongly dependent on the angle of operation and, in particular, the optimal operation is obtained at quasi-normal reflection (at angles between 0° and 15°). Such angular constrains are fulfilled by the spatial location of the subcomponents of the optoplasmonic module, in which i) the monolithic integration of the OLEDs onto the electrodes of the OPT guarantees a high degree of lateral proximity between the light emitting area and the detecting area (i.e. area between the two electrodes of the OPT), ii) the direct fabrication of the NPG onto the encapsulating glass of the chip favors an optimal vertical distance of the plasmonic component for reflection-mode detection.
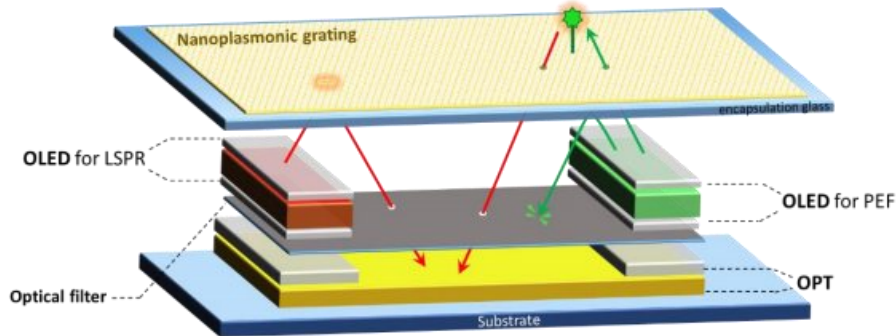
Figure 1. Schematics of the optoplasmonic module of the h-ALO sensor enabling both LSPR and PEF detection modes.

2.1 Nanoplasmonic Grating (NPG)

The sensing surface used within the h-ALO project is based on the nanoplasmonic grating (NPG) developed at Plasmore. This NPG presents several interesting features:

- it supports several plasmonic modes, either localized, propagating or mixed;
- since a transparent encapsulation glass is normally used as the substrate for the NPG, the plasmonic modes can be excited from the substrate side, allowing an easy integration of fluidic components on the top of the NPG and avoiding the incident light passing through the analysis liquid cell;
- no need of prism coupling, but possible integration on different substrate and optical components, to realize a compact and portable sensor, with a quasi-normal light-excitation and signal-collection geometry (maximized signal in LSPR detection mode);
- possible combination with additional detection techniques, such as PEF.

The NPG will be fabricated on the glass substrate used for the encapsulation of the photonic components before the assembling of the optoplasmonic chip. The fabrication protocol aims at nanostructuring a polymeric film (polymethyl methacrylate, PMMA), combining colloidal lithography and plasma-based processes to etch the colloidal mask and deposit a gold layer. The final structure is an optically thick gold film perforated by nanocavities of polymeric pillars arranged in a hexagonal lattice (Figure 2). This surface can be further functionalized with different coatings to favour the immobilization of biomolecules of interest.
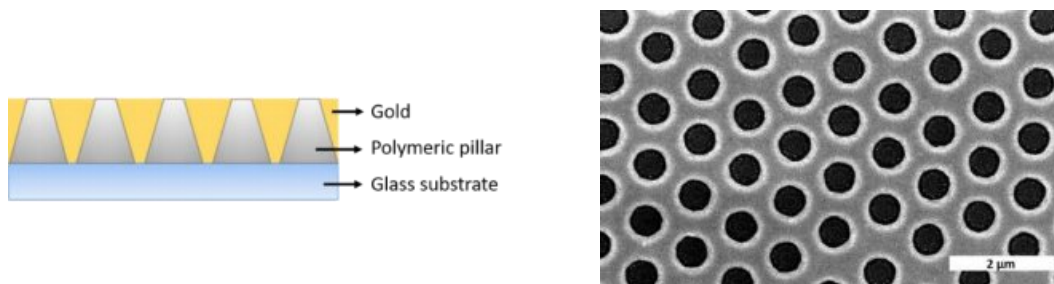
Figure 2. Side view of a simplified model of the nanoplasmonic grating (left); SEM image of the grating from top view (right).

The core detection principle of the optoplasmonic chip is based on Surface Plasmon Resonance (SPR). Specifically, the NPG detects refractive index changes occurring at the outer surface of the grating when it is in contact with different media, thus allowing the monitoring of biomolecular binding events. In particular, the sensing features of the grating rely on the presence of localized surface plasmon resonance (LSPR) modes related to the dielectric pillars. It was demonstrated, both theoretically and experimentally, that a tapered shape of the polymeric pillars allows to have an intense electric field strongly localized at the pillar top when the incident light impinges through the glass substrate side, leading to an improved surface sensitivity in virtue of a refractive index change occurring at the free surface of the grating.[1] Figure 3a shows the reflectance spectra of the NPG exposed to air and a buffer solution. It is worth noting the shift of the reflectance minimum when the medium on top of the NPG changes from air to a buffer solution. That shift is representative of a bulk refractive index change occurring at the NPG outer surface. Figure 3b represents the response of the grating to a small refractive index variation when the medium passes from a buffer to a test solution (i.e., a sucrose solution in buffer, at a defined concentration), which can be considered as an approximation of the surface sensitivity due to the LSPR. In details, Figure 3b shows the ratio of the reflectance spectra recorded when the NPG is exposed to the buffer and the test solutions, which is basically the sensitivity of the NPG to the solution of interest, *i.e.* the parameter to be monitored. For the h-ALO project, the structural features of the NPG have been already adjusted to make the LSPR sensing region matching the emission from the OLED for LSPR: since the highest sensitivity is typically obtained in the region between 700 and 900 nm, an effective coupling with the OLED emission is pursued at around 770 nm.

a)   b)
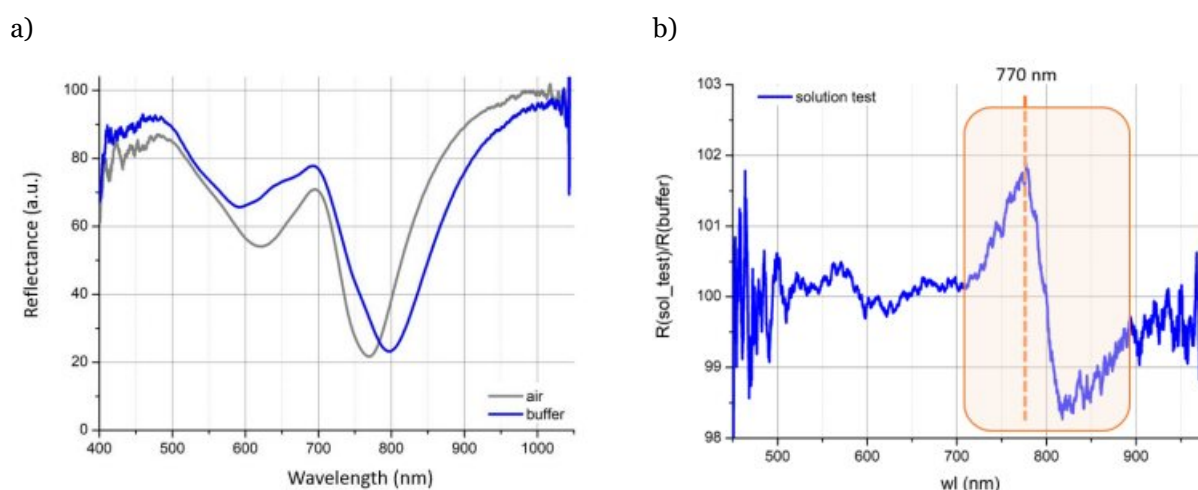
Figure 3. a) Reflectance spectra of the nanoplasmonic grating in air and in buffer; b) reflectance variation of the nanoplasmonic grating when the medium passes from buffer to a test solution with defined sucrose concentration. The spectral region of interest related to sensing in LSPR mode is evidenced by a rectangle.

As aforementioned, the use of a NPG allows the possibility to assess multimodal detection on the same sensing surface. Indeed, Plasmon Enanhaced Fluorescence (PEF) can be considered as an additional detection mode. The combined and synergic use on the same nanostructured surface of two different optical detection methods aims at overcoming the limits of each single technique and at improving the signal output, in terms of extended dynamic-range, high selectivity and high sensitivity in multiplexing format.

Figure 4 shows the reflectance spectra of the nanoplasmonic grating in buffer and two main minima are evidenced corresponding to spectral regions where a suitable plasmonic enhancement occurs. Different strategies can be considered to study the PEF effect, depending on the minimum selected to match the emission and/or excitation wavelength of the desired fluorophore.
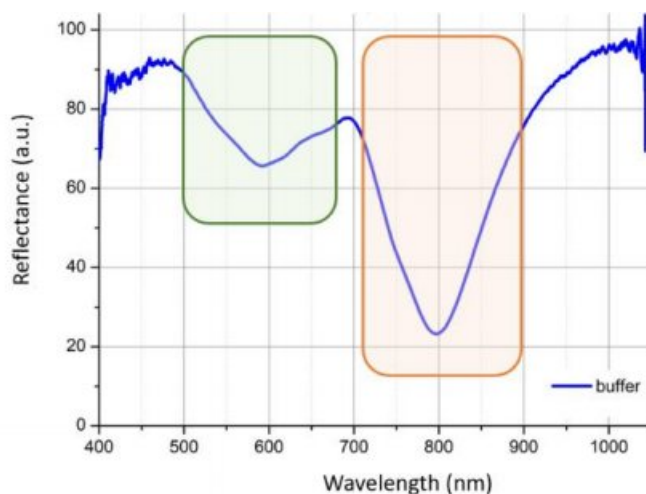
Figure 4. Reflectance response of the nanoplasmonic grating in buffer. The main regions to investigate the PEF effect are evidenced with green and orange rectangles.

The first option is to couple the fluorophore features with the plasmonic mode around 500-650 nm, but it is more difficult to be investigated because of the complexity of the contribution factors to that signal. The more promising strategy consists of matching with the LSPR region between 700 and 900 nm.

2.2 Light-emitting sources (OLEDs)

OLEDs are a well assessed light-emitting technology consisting in nanometer-thick devices based on a piled stack of organic layers. A host-guest blend, characterized by a high emission quantum yield, is typically incorporated in a sandwich-like structure between the anode and the cathode (Figure 5). Interlayers that fulfill a suitable energy alignment are also included between the electrodes and the emissive blend to guarantee an efficient charge-injection process from the electrodes to the emissive layer. Nowadays, the accurate selection of suitable materials allows the fabrication of highly efficient, and stable multicolor OLEDs.
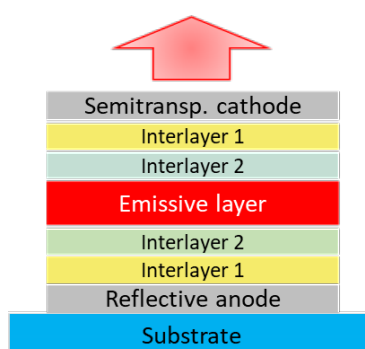
Figure 5. Schematic multi-layered structure of an OLED.

Aiming at the development of the optoplasmonic chip of the h-ALO sensor, two different OLEDs will be independently, and simultaneously, developed to guarantee the selective excitation of LSPR and PEF detection modalities (Figure 1). Specifically, materials, device structure, and emission characteristics of each of the two OLEDs need to be identified in strict correlation with the optical requirements of the NPG, the optically-selective OPT and the fluorophores (in the case of the PEF detection).
Based on the layout of the optoplasmonic chip (Figure 1), each OLED will be placed onto the optically selective OPT in correspondence of the source/drain electrode. According to that scheme, the OLED emission will

directly impinge at the NPG and hence top-emitting OLEDs need to be developed. Although they are already matter of discussion of the System-Engineering Work Group, the structural and operational characteristics of the OLEDs will be respectively provided in D1.4 and D1.5 at M20 and M24 respectively, together with the design of the optoplasmonic chip layout and the estimation of the expected signal.

The aim of this deliverable is instead the definition of the optical characteristics of the two OLEDs matching those of the other OPM's components. In particular, major focus is devoted to the selection of the emissive compounds that will comprised in the emissive layer of the OLED structures. The selection of the electrode interlayers will therefore follow the electronic properties of the selected emissive layer. All materials will be deposited by thermal sublimation by using fine metal masks to allow the obtainment of OLEDs fulfilling the pattern of integration of the optoplasmonic module.

2.2.1 OLED for LSPR

Given the spectral sensitivity of the NPG for LSPR detection (Figure 3), the OLED emission needs to overlap the spectral region 750 - 900 nm to ensure the chip operation. In this context, CNR and PLAS have a well-consolidated collaboration (EU H2020 project, MOLOKO – Grant Agreement n. 780839) on the development of LSPR sensing systems based on the combination of organic light-emitting devices and NPGs for the detection of contaminants in milk. Considering the promising results, we decided to use the same OLED structure for LSPR detection as that already used in the MOLOKO sensor. Specifically, a host:guest blend of an electrophosphorescent compound, i.e. Pt^{II}–tetraphenyltetrabenzoporphyrin [Pt(tpbp)], dispersed in a matrix of tris(8-hydroxyquinoline)aluminum (Alq_3) is selected as the OLED emissive layer for its strong near-infrared (NIR) emission at around 770 nm, which perfectly matches the maximum sensitivity of the NPG for LSPR detection (Figure 6). In addition to that, the typical Lambertian emission of OLEDs has been already proven to be compatible with the angular requirement of the LSPR detection of NPGs (Figure 6).
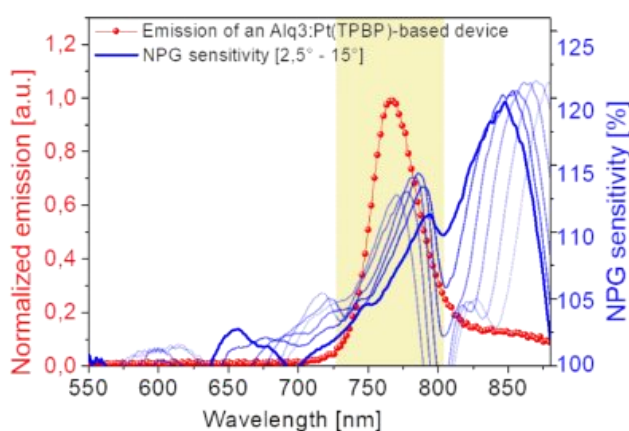
Figure 6. Normalized electroluminescence from an OLED based on a Pt(tpbp) emitter, peaked at around 770 nm, perfectly matching a relative maximum of sensitivity of the NPG for LSPR detection, at all angles included between 0° and 15°.

2.2.2 OLED for PEF

The PEF is a detection mechanism based on the enhancement of the emission from a fluorophore by means of the plasmonic characteristics of the NPG. The mechanism is enabled by the optical excitation and/or the emission of the fluorophore, which is bound to the outer surface of the NPG (Figure 1). It follows that the fluorophore will be optically excited by the light of the OLED, which first passes through the NPG. In order to guarantee a high efficiency in the PEF detection mode, a perfect spectral overlap of the OLED emission with the fluorophore absorption is therefore required. Nevertheless, a not-negligible intensity of the pristine OLED emission will be backscattered by the NPG towards the OPT. To improve the signal-to-noise ratio, the backscattered light will be hindered to reach the OPT by means of a suitable optical filter that is placed onto the OPT. It is therefore important that the emission spectrum of the OLED does not overlap with the fluorophore emission (Figure 7). This requirement involves a large spectral separation between the OLED

emission and the fluorophore emission, that can be also favored by a narrow bandwidth of emission of the OLED, *i.e.* a small full width at half maximum (FWHM). Typically, organic-based emitting sources as OLEDs are characterized by a large bandwidth of emission. Nevertheless, the device structure and the nature of the emissive compound are key factors to tune the FWHM of the electroluminescence spectra in OLEDs.

As listed in Table 1, a wide number of emitters covering the entire visible spectral region was analyzed in view of the OLED development for PEF detection.

A long list of commercial options was evaluated for deep-blue, blue, and green emission. It is worth mentioning that the use of unusual emitters involves the possible use of new interlayers and device structures, which may be poorly efficient for PEF detection. Widely used emitters would be therefore preferred.

Moreover, efficiency and stability of deep-blue and blue OLEDs are typically low.[2] Green, red and NIR emission are therefore preferred in view of the effective development of the h-ALO sensor.
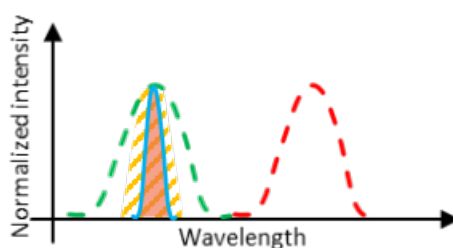
Figure 7. Ideal spectral characteristics pursued in the optoplasmonic module of the h-ALO sensor: dotted green and red lines refer to spectral absorption and emission of the fluorophore, respectively; the blue line refers to the emission spectrum of the OLED for PEF detection; the yellow region evidences the spectral characteristics of the optical filter; the orange area is the superposition between the OLED emission and the optical filter, thus highlighting that backscattered OLED light is blocked by the filter.

Table 1. Emitting host:guest materials, with corresponding spectral features, covering the entire visible spectral region evaluated for integration in OLED structures for PEF detection.

Emission	*Emissive host:guest*	*Emission peak [λ]*	*Full Width at Half Maximum*	**Provider**
Blue	BCPO:Firpic	485 nm	≈ 35 nm	Ossila
Blue	Cynora 009	483 nm	≈ 100 nm	Cynora
Blue	Cynora 001	474 nm	≈ 100 nm	Cynora
Blue	MADN:TBPe	≈ 460 nm ≈ 495 nm	≈ 80 nm	Ossila
Blue	DMAC-DPS	469 nm	-	Ossila
Blue	DPAVBi	474 nm	-	Ossila/Lumtec
Blue	FiR6	461 nm	-	Ossila
Blue	Host:BCzSB	427 nm 451 nm	-	Lumtec
Blue	Host:Mer-Ir(Pmb)3	415 nm	-	Lumtec
Blue	Host:Bepp2	445 nm	-	Lumtec
Blue	Host:DSA-Ph	459 nm 487 nm	-	Lumtec
Blue	Host:FIrN4	459 nm	-	Lumtec
Blue	Host:Fac-Ir(Pmb)3	405 nm	-	Lumtec

Blue	Host:BSB4	424 nm 444 nm	-	Lumtec
Blue	Host:Ban-(3,5)-CF3	440 nm	-	Lumtec
Blue	Host:PCAN	441 nm	-	Lumtec
Blue	Host:FK306	454 nm	-	Lumtec
Blue	Host:BNP3FL	437 nm	-	Lumtec
Blue	Host:BCzVBi	438 nm	-	Lumtec
Blue	Host:BCzVB	441 nm 462 nm	-	Lumtec
Green	TCTA:Ir(ppy)$_3$	520 nm	≈ 40 nm	Sigma Aldrich
Green	Alq$_3$:C545T	525 nm	-	Lumtec
Green	Host:Ir(ppy)$_2$(bpmp)	519 nm	-	Ossila
Green	TAZ:Ir(ppy)$_2$(acac)	520 nm	-	Ossila
Red	Bebq2:Ir(dmpq)$_2$(acac)	609-620 nm	-	Ossila
Red	Host:Ir(MDQ)2(acac)	600 nm	-	Ossila
Red	Alq$_3$:Ir(piq)$_3$	626 nm	≈ 50 nm	Sigma Aldrich
Red	Alq$_3$:Pt(OEP)	650 nm	≈ 10 nm	Sigma Aldrich
Red-NIR	Alq$_3$:Pt(TPBP)	770 nm	≈ 20 nm	Lumtec

2.3 Light-sensing component (OPT)

In the optoplasmonic module, the light-sensing component is the optically selective Organic Phototransistor (OPT). Within light detectors, OPTs compared to organic photodiodes (OPDs) allow to exploit the intrinsic switching and amplifying functionality of transistors for maximized signal-to-noise ratio, which is particularly relevant for low-intensity signals (i.e. for analytes in very low concentration). In addition, the general feature of organic transistors of having electrodes in a co-planar geometry and the light sensing area fully exposed, allows for the facilitated integration of the other optical and optoelectronic components, such as the optical filter and the light sources (OLEDs), and operation at quasi-normal incidence (for optimized LSPR detection).

The optical requirements of the optically selective OPT should enable LSPR and PEF detection. Therefore, the opticqlly selective OPT should have a high response which matches both the spectral region of the electroluminescence from the OLED for LSPR, and with that of the Fluorophore emission for PEF. In addition, any backscattered excitation light from the OLED devoted to PEF should be not detected. To this aim, an optical filter is integrated onto the OPT that will be then selectively sensitive only in the spectral region of LSPR and PEF signals (optically selective OPT). The specifications on the optical filter are mainly correlated with those of the light sources (OLEDw) and of the fluorophores, and are discussed more in detail in Section 4.

For better matching multiple requirements, and in particular to separately optimize (as much as possible) the optical requirements from the operational requirements to improve the collected photocurrent (output signal in the optoplasmonic module), we choose a specific bilayer architecture for the OPT (Figure 8). In this architecture, an organic photoactive layer is placed on top of a field effect semiconductor, so that the light absorption and photoinduced-charges separation processes, and lateral charge transport occur in the top layer and in the bottom layer respectively, and can be optimized separately. This architecture offers a great potential for broadband light detection. Also, this allows the simultaneous optimization of both photo-responsivity and sensitivity, which are the two most significant Figures-of-Merit correlated to PEF and LSPR detection respectively.
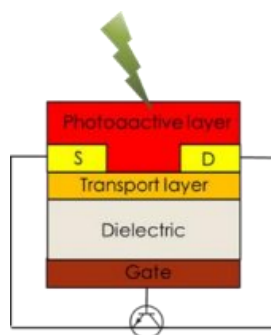
Figure 8. Schematic side view of a OPT with bilayer architecture.

The preferred spectral region for LSPR, according to the characteristics of the NPG, is around 770nm, in the NIR (see Section 2.2.1): the OLED for LSPR emits light at around 770 nm, matching the main peak of reflection of the NPG. For PEF instead, the spectral region of interest depends on the selected Fluorophore(s). According to D1.2 the final selection includes fluorophores whose emission spans from 520 to 820 nm. Accordingly, an OPT with a high External Quantum Efficiency (EQE) in the spectral range 520 - 820 nm is a secure option.

Literature reports on a variety of materials which could be possibly used as light absorbing materials (photoactive layer) in the OPT.[3] To further enhance the photoinduced charge separation efficiency in the photoactive layer, especially for excitons with a large binding energy as it is in organic materials, one of the best options is to combine two materials with different electron affinity into a bulk heterojunction (BHJ) photoactive layer. In a BHJ photoactive layer with interpenetrated domains, one material traps one type of charges, while the other material injects charges with the opposite sign into the field effect layer (channel), provided the energetically favored alignment of the energy levels between the two materials/layers. In this way, a more efficient unipolar charge transport is achieved (up to five orders of magnitude difference in electron and hole mobility can be reached). Hence, a continuous flow of the photogenerated holes (or electrons) is ensured along the channel for a significant duration before being recombined with trapped electrons (or holes), and a high photocurrent gain (up to 10^5) can be obtained. This enables the boost of both responsivity (up to 10^5 A W^{-1}) and sensitivity (light-to-dark current ratio 10^4 - 10^5 for nW cm^{-2} - mW cm^{-2} illumination).

Two possible material options selected for the bulk heterojunction (BHJ) photoactive layer of the OPT, sensitive in the spectral range 520 - 820 nm, are reported in Figure 9, together with their expected spectral response.
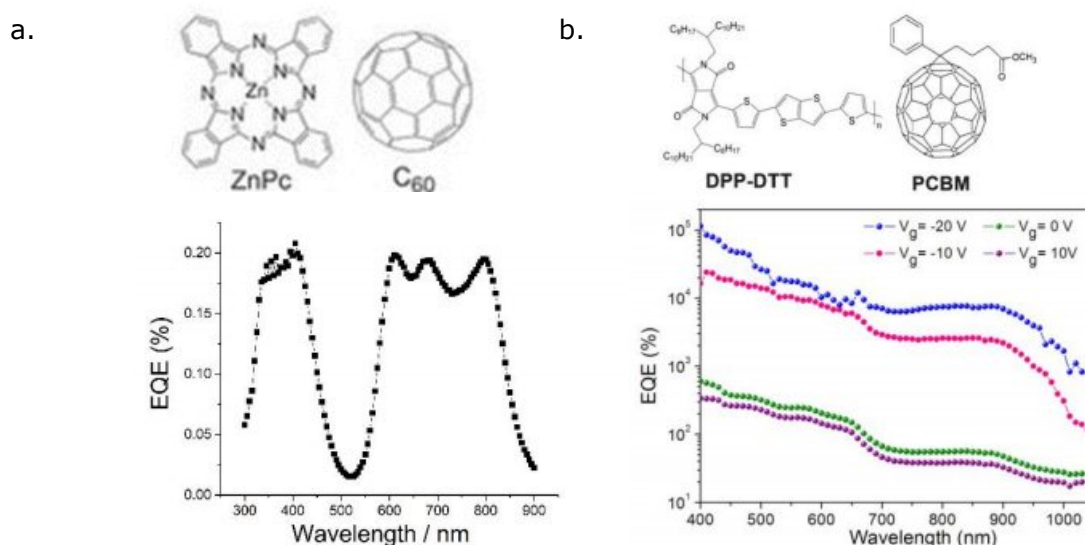
Figure 9. Material options selected for the bulk heterojunction (BHJ) photoactive layer of the OPT, with corresponding spectral response.

In option (a) of Figure 9, the BHJ photoactive layer is based on Zn-Phthalocyanine (ZnPc, donor material) and Buckminster fullerene (C60, acceptor). OPDs based on such BHJ, easily deposited by vacuum thermal evaporation, have already been successfully fabricated and employed by CNR in a previous project (EU H2020 project, MOLOKO – Grant Agreement n. 780839) and demonstrated a suitable spectral response for LSPR detection, when the NPG defined in Section 2.1 and the OLED for LSPR defined in Section 2.2 are employed.

Patterning of the ZnPC:C60 photoactive layer can occur by using fine metal masks, to allow the alignment with the field effect channel and source and drain electrodes, and to allow fulfilling the overall pattern of integration of the optoplasmonic module.

The external quantum efficiency EQE (also called incident photon to collected electron efficiency, IPCE) of a characteristic OPD fabricated at CNR and based on ZnPC:C60 photoactive layer shows the highest EQE (above 10%) between 550 and 850 nm (bottom panel of Figure 9a), ensuring spectral overlap with light signals in both LSPR and PEF modes. To note, the absolute value of the EQE is typically increased above 100% in OPTs, thanks to the above cited photocurrent gain effect.

In option (b) of Figure 9, the BHJ photoactive layer is based on a low band gap p-type co-polymer Poly[2,5-(2-octyldodecyl)-3,6-diketopyrrolopyrrole-alt-5,5-(2,5-di(thien-2-yl)thieno [3,2-b]thiophene)], or DPPDTT, and a derivative of Buckminster fullerene, [6,6]-phenyl-C_{61}-butyric acid methyl ester, or PCBM. The DPPDTT:PCBM photoactive layer can be easily deposited from solution in organic solvents, and patterned by mechanical scratching or photo-patterning.

OPTs based on such BHJ, in a single-layer architecture, have already been reported in literature, showing amongst the highest responsivity in the NIR spectral region.[4] In detail, an EQE up to 10^4% in the 400-900 nm spectral region is reported (bottom panel of Figure 9b).

To be employed in an OPT geometry, suitable HOMO or LUMO alignment with the field effect channel should be accomplished. Given that DPPDTT and ZnPc, PCBM and C60 show the same HOMO and LUMO levels respectively, the energetic requirements for the field effect material are the same as reported above for ZnPc:C60.

In both cases of either a ZnPc:C60 or a DPPDTT:PCBM based photoactive layer, the field-effect charge transport bottom layer of the OPT should have a suitable alignment of the energy levels and a high field effect mobility. Table 2 reports some possible field-effect materials options for the OPT, with main electrical and energetic characteristics, and processing conditions.

Table 2. Material options selected for the field-effect charge transport layer of the OPT, with corresponding electrical and energetic characteristics, and processing conditions.

Material (commercial name)	Chemical name	Field effect mobility (n- or p- type, cm² V⁻¹ s⁻¹)	Processing conditions	HOMO/ LUMO (eV)	Ref
C8-BTBT	2,7-Dioctyl[1]benzothieno[3,2-b][1]benzothiophene	μ_p, 0.2 ÷ 1	Thermal sublimationin high vacuum	-1.7 / -5.5	5
Tips-pentacene	6,13-Bis(triisopropylsilylethynyl)pentacene	μ_p, 0.2 ÷ 0.7	Thermal sublimationin high vacuum	-3.5 / -5.4	6
DPPDTT	Poly[2,5-(2-octyldodecyl)-3,6-diketopyrrolopyrrole-alt-5,5-(2,5-di(thien-2-yl)thieno [3,2-b]thiophene)]	μ_p, 0.2 ÷ 1 μ_n, 0.06	Spin coating from solution of organic solvents	-3.5 / -5.2	4, 7
IZO	Indium Zinc Oxide	μ_n, 3 ÷ 20	Spin coating, sol-gel	-4.3 / -7.5	8
IGZO	Indium Gallium Zinc Oxide	μ_n, 10 ÷ 20	Radio-frequency sputtering	-4.5 / -8.0	9

Concerning the other layers which compose the OPT (i.e. the gate electrode, the dielectric, possible interlayers), which only have an influence on the operational conditions and geometry of the OPT rather than on the spectral characteristics, they are already matter of discussion in the System-Engineering Work Group. Such layers/materials and geometry will be defined later in D1.4 (due at M20) and D1.5 (due at M24), in conjunction with the design of the optoplasmonic module layout and the estimation of the expected signal.

3 Calculations for the best spectral matching of OLEDs, NPG and fluorophores

Fluorescence efficiency is depending on two, non-correlated processes: i) the excitation efficiency concerning, in our case, how efficiently the light emitted by the OLED may excite the Fluorophore, and ii) the emission efficiency which is depending on the quantum efficiency of the emitting Fluorophore, but also on the interaction of the Fluorophore with the environment and, in particular, with the NPG.

In order to calculate the combined response of the source (OLED), the Fluorophore and the active surface (NPG), we analyzed separately the two processes starting from the specific figures of merit of each component and then we compared the performance of the different possible combinations of components to choose the best ones.

We started by considering the final list of Fluorophores proposed in D1.2:

- NIR 820
- ATTO611x
- Chromeo P503
- ATTO490LS
- FM1_43
- BBD
- Dye524
- NBDx

A few other Fluorophores of the ATTO and AlexaFluor series have been added because they appeared particularly suited for biofunctionalization process, although presenting a Stokes Shift smaller than 60 nm and in a few cases a Quantum Yield below 0.3 (Table 3).

Table 3. Fluorophores of the ATTO and AlexaFluor series added to the final list, together with their corresponding spectral/optical Figures-of-Merit.

Fluorophore	Abs/Exc. max (nm)	Em. max (nm)	Stokes Shift (nm)	Molar Extinction Coefficient (mol⁻¹·cm⁻¹)	Quantum Yield
Alexa Fluor 750	749	775	26	290000	0.12
ATTO620	620	644	24	120000	0.5
ATTO740	740	764	24	120000	0.1
ATTO700	700	720	20	120000	0.25

To note, in the case of these additional fluorophores, issues may arise due to their small Stokes Shift: a spectral overlap could indeed occur between the emission of the OLED and the emission of the fluorophore, as a consequence of the typically large bandwidth of the OLED emission. This fact would reduce the signal-to-noise ratio and it would make difficult the design of an optimal optical filter (with very steep absorption band edge). More details are given in Section 4.

Therefore, it is important that an efficient fluorophore excitation (i.e. good spectral match between the OLED emission and the fluorophore absorption) is guaranteed by minimizing the spectral overlap between the OLED emission and the fluorophore emission spectra. Accordingly, a pre-selection of OLED emitters was done by

rough estimation of their spectral superposition with the fluorophores' emission spectra. Then, a detailed comparative analysis was done on the following short list of OLED emitters, which are all highly performing:

- Blue OLED based on TBPe guest emitter
- Blue OLED based on Firpic guest emitter
- Green OLED based on Ir(ppy)$_3$ guest emitter
- Red OLED based on Ir(piq)$_3$ guest emitter
- Red OLED based on Pt(OEP) guest emitter
- Red OLED based on Pt(TPBP) guest emitter

Figures 10 shows the normalized absorption spectra of the selected Fluorophores superposed to the emission spectrum of each OLED (thick curve). The area of the overlap between spectra is the useful fraction of excitation of the Fluorophore in relation to the OLED emission.
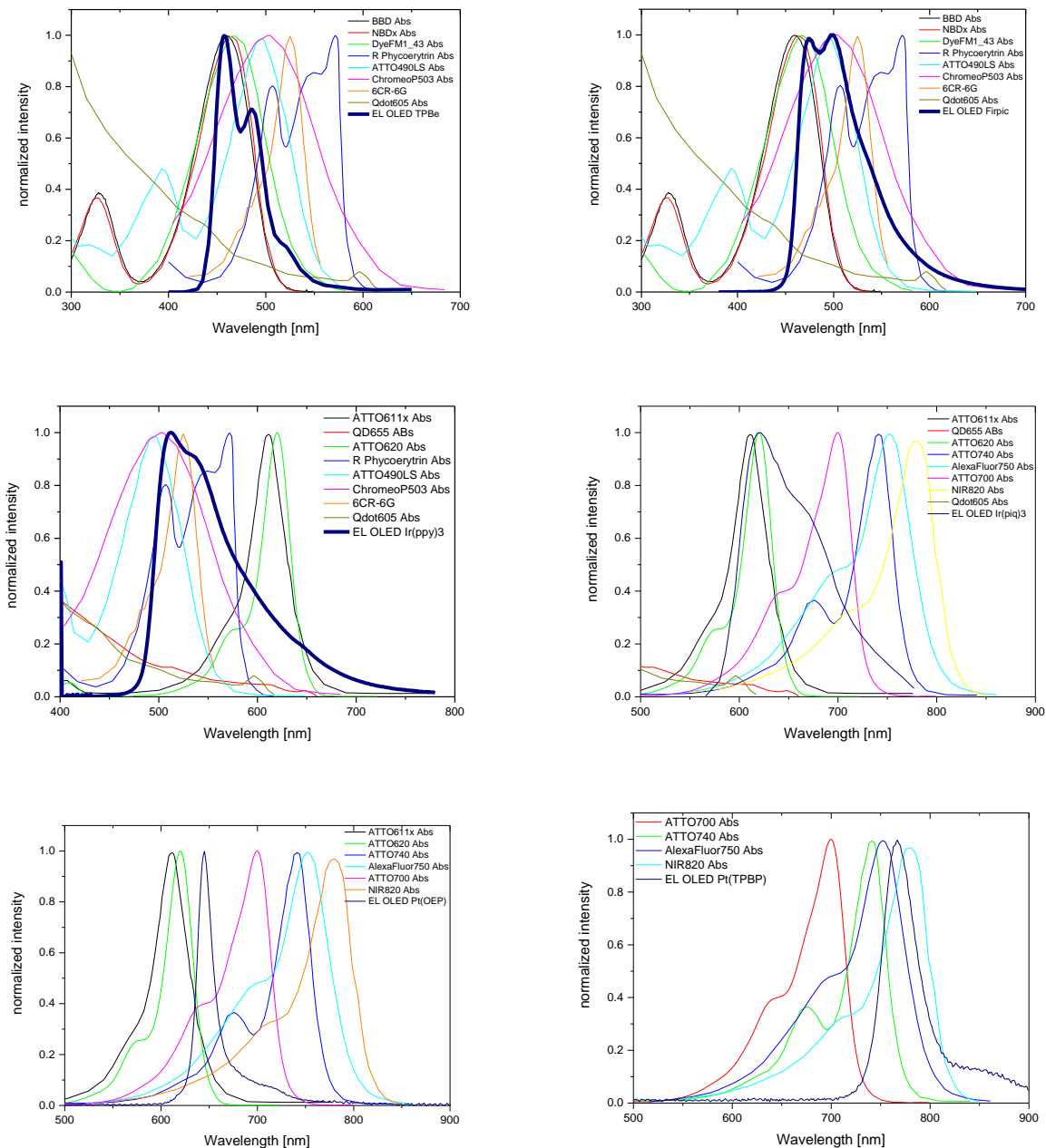
Figure 10. Normalized absorption spectra of the different dyes compared with the normalized emission spectrum of each of the selected OLED (thick curve of each panel).

The effective absorption can be evaluated as the integral of the curve obtained by the product of the OLED emission spectrum and the Fluorophore absorption spectrum once weighted by the Fluorophore's extinction coefficient.

To complete the evaluation of the excitation efficiency, one has to consider the effect of the reflectance/transmittance, and the correlated plasmonic effects, of the NPG since the light emitted by the OLED must pass through the NPG before reaching the Fluorophore. According to the literature, a metallic grating can act as an antenna enhancing, in the proximity of the surface, the electric field of an impinging electromagnetic wave. The enhancement of the excitation rate due to the antenna effect with respect to the excitation without antenna is given by the ratio of the excitation efficiencies (γ and γ_o):[10]

$$\gamma_{exc} / \gamma_{0exc} = |E|^2 / |E_0|^2$$

where E and E_o are the electric field intensities with and without antenna effect, respectively.

An estimate of the field enhancement is obtained by finite-difference time-domain method (FDTD) simulation method applied to simulate the optical response of the NPG. For such purpose, the commercial FDTD simulation suite Lumerical (2021 Ansys Canada Ltd.) is used. The hexagonal grating of polymeric pillars embedded into a gold layer has been modeled as sketched in Figure 2. As final check, simulated results are compared with the available experimental data of the NPG optical characterization.

The simulation results to well reproduce the main features that are common to all the samples produced by PLASM. In particular, a deep minimum appeared in the reflectance in correspondence to the main plasmonic resonance (and to a maximum in the transmittance spectrum). At shorter wavelengths, a reflectance maximum (transmittance spectrum minimum) occurred, followed by a further intensity decrease.

Figure 11 shows the result obtained for a structure with pitch of 450 nm, 150 nm thick and a pillar radius of 100 nm at the top and 120 nm at the basis.
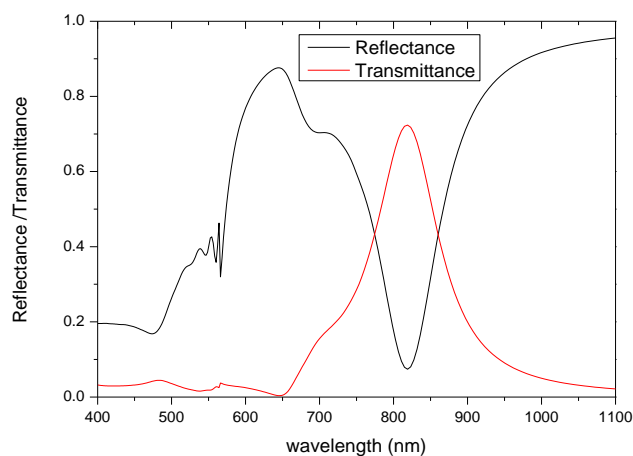
Figure 11. Simulated reflectance and transmittance spectra of a grating structure of polymeric cones embedded into a gold layer.

The corresponding field intensity at the top of the pillar, where the distribution of Fluorophore molecules is expected to occur, is presented in Figure 12. One can notice that the general behavior is resembling the one of the transmittance spectrum in Figure 11. Specifically, an enhancement region is evident in correspondence of the plasmonic features, and some other regions, *i.e.* the minimum at around 650 nm, are related to the suppression of the field. To note, the relevant enhancement concerns the region above the pillar. Diversely, the field distribution is not homogeneous over the surface (region with no pillars).

In order to have a simulation closer to the experimental conditions, we simulate the Absorbance (A) of a thin layer (10 nm) of a hypothetical absorbing material with a constant extinction coefficient over the whole spectrum. The observable A is obtained by calculating the Reflectance (R) and the Transmittance (T) of two structures respectively with and without such an absorbing layer, according to the analytical relation A=1-R-T. The difference between Absorbance with and without the absorbing layer provides a spectrum related to the

bare absorption layer, cancelling the large absorption contribution due to the metallic components. The result is shown in Figure 13.
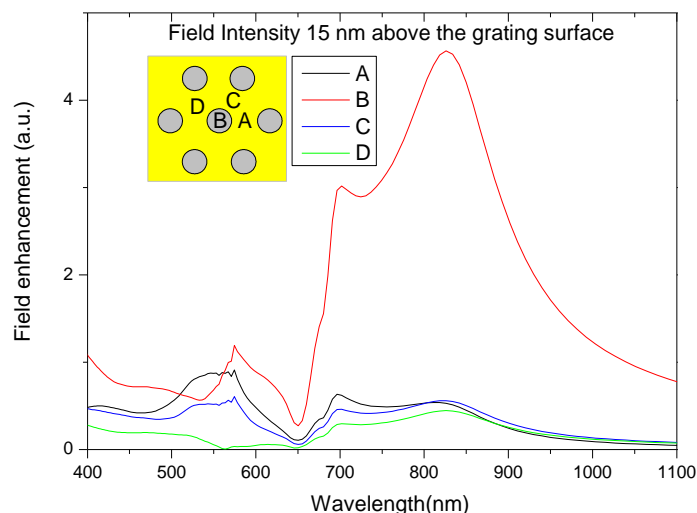
Figure 12. Electric field intensity at 15 nm over the surface with respect to the one simulated without grating. The curves refer to different positions with respect to the pillar configuration.
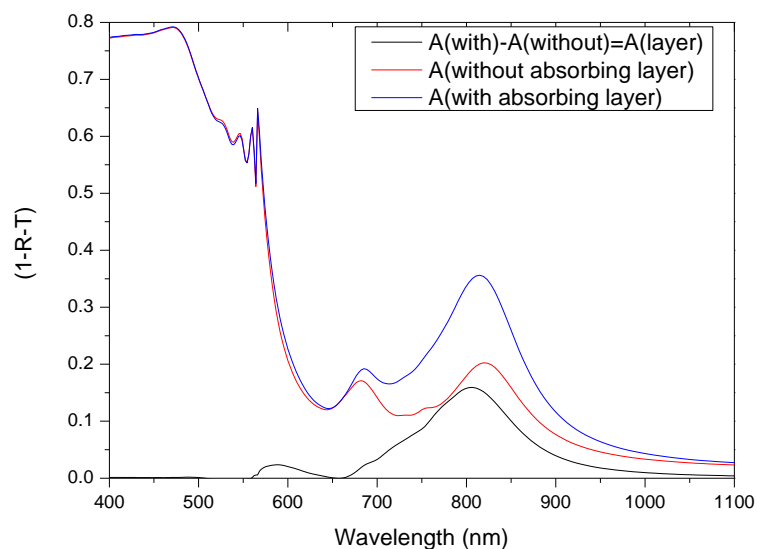
Figure 13. Absorbance spectra of a grating with or without a 10 nm-thick absorbing layer over the NPG surface.

The resulting absorption spectrum of the absorbing layer on top of the NPG layer exhibits the same spectral features of the electric field at the NPG. It is immediately evident that, due to the strong absorption of gold at the lowest wavelengths, no important contribution is obtained below 550 nm. Thus, this portion of the visible spectrum has a poor relevance for the activation of PEF.

Then, in order to compare the Fluorophores' performance, we calculate a parameter, named as Excitation coefficient, which corresponds to the integral of the curve obtained by multiplying i) the normalized Fluorophore's absorbance spectrum (Figure 10), ii) the OLED emission spectrum (Figure 10), iii) the above-obtained Absorbance spectrum of the absorbing layer (Figure 13) and iv) the extinction coefficient of the grating, weighted by the extinction coefficient of each Fluorophore. Results are shown in the Table 4.

Table 4. Efficiency parameters used to select the fluorophores.

OLED emitter for PEF	Fluorophore	Excitation coefficient	Emission coefficient	PEF factor
TPBe	BBD	0.74629		--
	NBDx	0.86056		--
	DyeFM1_43	1.80436	0.81072	1.46283
	R Phycoerytrin	38.13158	1.14979	43.84317
	ATTO490LS	1.49714	4.44097	6.64875
	ChromeoP503	1.13408	1.39811	1.58556
	Dye 524	1.23329	--	--
Firpic	BBD	0.66967	--	--
	NBDx	0.80226	--	--
	DyeFM1_43	1.91157	0.81072	1.54974
	R Phycoerytrin	146.5003	1.14979	168.44403
	ATTO490LS	2.0066	4.44097	8.91124
	ChromeoP503	2.13715	1.39811	2.98796
	Dye 524	1.71286	--	--
Ir(ppy)$_3$	ATTO611x	26.86917	5.5844	150.04827
	ATTO620	23.93557	2.4614	58.91505
	R Phycoerytrin	314.76218	1.14979	361.90923
	ATTO490LS	0.89456	4.44097	3.97272
	ChromeoP503	3.2045	1.39811	4.48023
	Dye524carboxyrhodamine6G	0.54878	--	--
Ir(piq)$_3$	ATTO611x Abs	41.57343	5.5844	232.16278
	ATTO620 Abs	41.5165	2.4614	102.18879
	ATTO740 Abs	82.18962	2.71412	223.07235
	AlexaFluor750 Abs	242.11162	3.31909	803.58974
	ATTO700 Abs	76.50902	4.54371	347.63489
	NIR820 Abs	97.03278	2.06663	200.53066
Pt(OEP)	Alexa 750	55.06458	3.31909	182.76418
	Atto700	16.32821	4.54371	74.19066
	Atto 740	17.113	2.71412	46.4467
	Atto 611	2.79241	5.5844	15.59392
	Atto 620	3.06227	2.4614	7.53747
Pt(TPBP)	ATTO700 Abs	6.54875	4.54371	29.75562
	ATTO740 Abs	151.94471	2.71412	412.39591
	AlexaFluor750 Abs	909.40464	3.31909	3018.39392
	NIR820 Abs	753.04066	2.06663	1556.25487

To complete our analysis, we must consider the emission capacity of each Fluorophore combined with a possible quantum yield enhancement by the NPG, and the collection capability and efficiency in our configuration. One has to consider that the OPT is collecting the fluorescence signal from the glass side of the grating, whereas the Fluorophore emission is occurring on the external surface of the NPG. Then, emitted light must travel through the grating (thickness in the order of a few hundreds of nanometers) to reach the OPT detector. Therefore, a rough but effective evaluation of the possible optical loss due to the presence of the grating in the optical path can be obtained by multiplying the emission spectrum of each Fluorophore by the spectral transmittance of the grating. The integral of the so obtained curve weighted by the quantum yield of the fluorophore is the second parameter to consider, and it is listed in the fourth column of Table 4 (Emission Coefficient). By combining Excitation and Emission coefficients, we can evaluate the global efficiency of the different OLED-Fluorophore-NPG configurations. Indeed, t6he last column in Table 4 shows the product of the previous excitation ad emission coefficients, thus leading to the so-called PEF factor. The reported PEF factor is an indicator to draft a first ranking for all the analysed OLED-fluorophore couples, based on their spectral features and optical figures of merit.

Some further considerations should be also taken into account:

1) Despite the combinations of fluorophores with the TPBP-based OLED have the best PEF coefficients among all, that OLED emitter has been already selected for the LSPR detection mode. Different spectral regions (and different OLED emitters) must be selected for the PEF and the LSPR detection modes. Indeed, if using the same OLED, the optical filter necessary to cut the backscattered light of excitation of PEF would impede the LSPR signal to reach the OPT (Figure 1).

2) According to Deliverable 1.2, only some of optically effective Fluorophores here considered in the calculations can be bio-functionalized (chemically coupled to the 5' and 3' ends of DNA oligonucleotide strands). As a result, a shortened list of fluorophores of interest is drafted. It includes:

- AlexaFluor 750
- ATTO 740
- ATTO 700
- ATTO 620
- ATTO 490LS

3) The OLED emission and the fluorophore emission spectra must be separated (minimal overlap) to facilitate the development of the optical filter. In addition to that, the spectral range of interest for PEF must be compatible with that of LSPR (766 nm ± 20 nm), and in particular it should be so that to avoid the need for optical filters cutting light > 750 nm, given that LSPR detection occurs at 766 nm ± 20 nm.

By considering the calculations of the PEF efficiency together with the further observations reported above, in the following best OLED-fluorophore combinations are highlighted:

- OLED (Ir(piq)3) – AlexaFluor 750   [PEF factor = 803]
- OLED (Ir(piq)3) – ATTO 700   [PEF factor = 347]
- OLED (Ir(piq)3) – ATTO 740   [PEF factor = 223]
- OLED (Pt(OEP)) – AlexaFluor 750   [PEF factor = 182]
- OLED (Ir(ppy)3) – ATTO 620   [PEF factor = 58.9]

Best combinations are ranked by the PEF factor values, which is a first indicator of the PEF efficiency: high values suggest higher efficiencies with respect to other OLED-fluorophore combinations.
However, as a final remark, some further issues could be also considered for improving the accuracy of calculations.

First, the use of the quasi-normal transmittance is well suited for light generated and detected far from the NPG surface, but it is neglecting other out-of-normal components, as well as the interaction of the Fluorophore emission with the NPG surface. Actually, the Fluorophore molecule is considered as a Lambertian source. For a more in-depth evaluation of the emission-angle dependence, a model refinement including the angular emission could be further performed. In the model refinement, the Fluorophore will be considered as a dipole emitter in order to consider the different orientation of the molecule over the NPG surface. Preliminary simulations indeed evidenced a spectral modification of the light transmitted by the NPG and directed to the OPT. In addition to that, a slight dependence on the distance of the Fluorophore from the surface has been noticed, thus suggesting that an optimization of such a distance can be also played.

In the selection of the best OLED-Fluorophore combination, the intensity of the OLED emission is a parameter to consider. A reliable comparison between the intensity of emission of OLEDs based on Ir(piq)$_3$ and Pt(OEP) emitters is difficult to be done by taking values from literature, because of the diversity of the device structures. From general considerations on their quantum yields of emission, both emitters are high performing. However, a slightly higher performance is expected from OLED based on Ir(piq)$_3$.

Regarding the OPT, a constant response over the whole spectrum must be considered, according to the EQE spectra taken from the literature (Figure 9).

The reported considerations will be included in a more detailed analysis about the entire optoplasmonic module. Therefore, Table 4 will be refined and then updated by including the optical power of OLEDs and the EQE of the OPT to estimate the signal expected for LSPR and PEF detection modes. Results will be reported in the description of the integrated chip (D1.4 at M20 and D1.5 at M24).

4 Optical filters for the best combinations of OLEDs, NPG and fluorophores

For the development of the optoplasmonic chip, the integration of an optical filter element is necessary for the fluorescence detection mode, in order to block excitation light from reaching the light detector (the OPT), which is not intrinsically spectrally selective, so to obtain an optically selective OPT. In addition, since in the current configuration of the optoplasmonic module, a reflection mode is used for plasmonic and fluorescence detection, and the same OPT is used for both detection modes (Figure 1), the optical filter should fulfill optical requirements compatible with both detection modes.

Since the filter is placed on top of the OPT, it is necessary to firstly check the compatibility of fabrication processes of filters with the OPT technology. In the case of sputtering, high-vacuum sublimation, atomic layer deposition (ALD) or chemical vapor deposition (CVD), the deposition process needs to be realized at a temperature sufficiently low to avoid thermal degradation of the photoactive layer of the OPT. In the case of solution processing, the solvent from which the optical-filter material(s) are deposited should be orthogonal to the one eventually used for depositing the underlying photoactive layer of the OPT, or in any case it should not dissolve it. For broadening the library of possible solvents to be used, electrically inert and transparent layers (i.e. solution processed CYTOP polymer that can be processed at CN) can be deposited on top of the OPT before the deposition of the optical filter, to protect the photoactive layer from solvents or highly reactive atoms/molecules.

Regarding their optical features, the filters are typically defined by the following figures of merit:

- the band-edge position
- the absorption edge width
- the % of transmittance (T%) in the spectral region of emission of the fluorophore of interest, and % rejection (R%) in the spectral range of the emission of the OLED
- the angle dependency of T% and R%

Since the filter must be placed on top of the OPT for both PEF and LSPR detection modes, a first requirement is a band edge positioning at a wavelength shorter than the working wavelength for LSPR (below 770 nm).

For PEF, depending on the selected OLED/fluorophore combination, the optimal band-edge position changes (Figure 14). Also, the absorption edge width (that is the projection on the wavelegth axis of the absorption edge) has to be smaller than the difference between electroluminescence spectrum peak of the OLED and the fluorescence spectrum peak of the fluorophore (that is the spectral shift: peak-to-peak spectral offset). To note, even though for most of the selected OLED-fluorophore combinations ranked in Section 3 there are large peak-to-peak spectral offset, their emission spectra still partially overlap. Therefore, an optical filter with a small absorption edge width and finely tunable band edge position (in accordance with the OLED-fluorophore combination) must be designed.
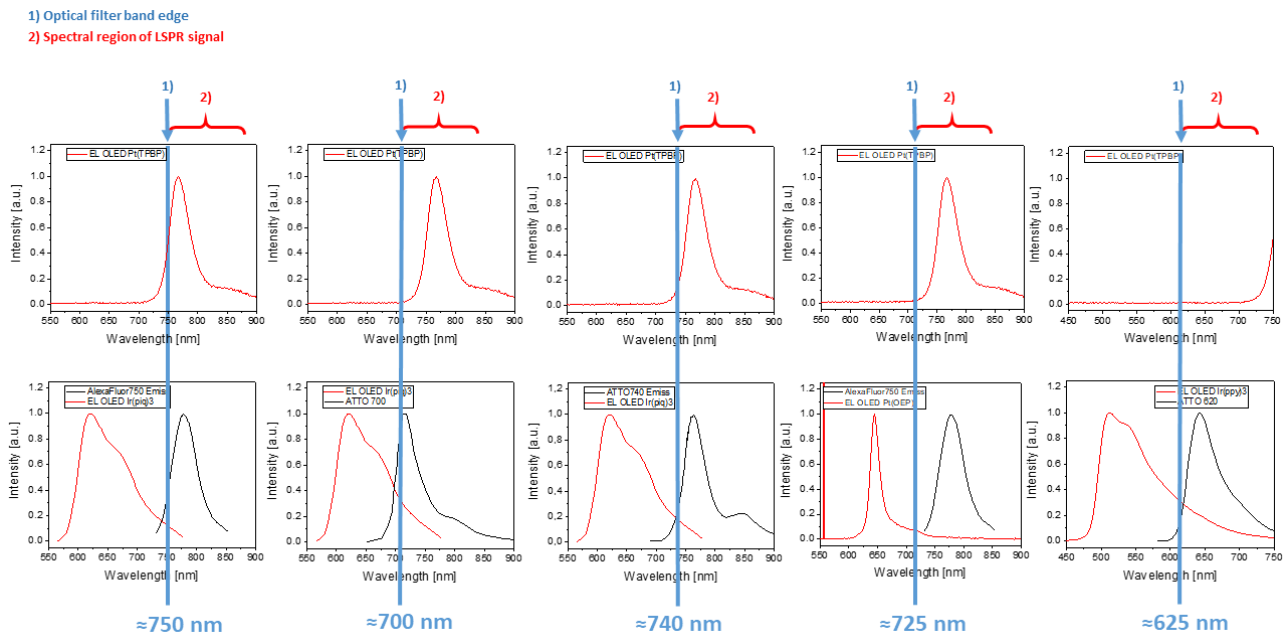
Figure 14. Requirements of band-edge position of the optical filters in relation to the selected OLED-fluorophore combination for PEF, and with the LSPR signal.

The required T% and R% of the optical filter should be ideally maximized. A more careful evaluation of their effect on the overall signal estimation, for both PEF and LSPR, will be given in the Task 1.4, i.e. System-engineering for a functional prototype.

Finally, the optical filter ought to show no significant changes of optical features with the light-impinging angle, or such change should be compatible with the angular requirements of the LSPR detection of NPGs (in the range from the normal incidence at 0° to +/-15°, Figure 6).

Typical optical filter technologies include absorption filters and interference filters.[11] These two main options are presented below, together with their advantages/disadvantages, both in terms of figures of merit and of processing conditions, for their integration onto the OPT. The best options are finally selected for being implemented within WP2, Task 2.2, "Spectrally-selective organic/hybrid transistors for light sensing (M2 – M12).

4.1 Absorption filters options

One advantage of absorption filters based on organic materials (aggregated chromophores, or chromophores embedded in a transparent/inert polymeric matrix, or colored polymers) is that they can be processed at low temperature and patterned easily and at low cost.

Organic absorption filters have a thickness ranging from a few - tents of micromiters (pure chromophoric) up to millimiters (chromophore-loaded polymers). Such filters are able to give a R% up to 99.9999% in the excitation light range, and a T% of around 40% in the fluorophore's emission region. Other advantages of organic absorption filters is that, unlike interference filters, their response is independent from the angle of incidence.

The main disadvantages of organic absorption filters are:

i) the typically large absorption edge width (>30 nm, larger compared to interference filters)

ii) 100% transmittance in the fluorophore's emission region is hard to be achieved, when a high R% of excitation light is required; this is a possible issue for assays with low fluorophore concentrations;

iii) since targeted band-edge position is determined primarily by the material properties, it could be hard to find a compromise between a finely tuned band-edge position and compatible processing conditions for integration;

iv) self-fluorescence from the filter can occur, interfering with fluorescence from the assay; again, this is a possible issue for assays with low fluorophore concentrations.

To overcome the self-fluorescence, filters designed by the group of Prof. J. De Mello can be a possible solution.[12] Such kind of filters rely on absorption filtering by an organic dye, which is adsorbed onto a mesoporous titanium oxide thin film. The titanium oxide thin film acts as a quenching site, strongly reducing self-fluorescence from the dye without perturbing its absorption characteristics. However, while the titanium oxide layer can be processed from solution at a relatively low temperature (around 120°C), dye absorption occurs by dip-coating, which is a process potentially detrimental for the performance of the whole OPT, when optical filter has to be directly integrated on top of it to produce the optically selective OPT.

4.2 Interference filters options

Depending on the type of filter (long pass, short pass, band pass, notch filter, ...), interference optical filters can be realized using different technologies. Since the excitation wavelength for fluorescence detection is shorter than the emission wavelength, for the given setup either a notch or long-pass filter will be necessary in order to block the excitation wavelengths of PEF and to transmit the LSPR signal.

For the realization of these filters, two methods are considered. In details, the described methods can be implemented by partners of the consortium:

1. Multilayered stacks of nanometer-thin layers of conductive and dielectric materials (typically at least 10 layers). The materials are usually deposited in high vacuum through physical (PVD) or chemical vapor deposition (CVD) methods, but also solution processing (in the case of polymeric materials) is possible
2. Sub-wavelength structures of metals and dielectrics. The filters consist of regular grids of either openings or pillars of the active materials. Usually the filters are realized by just one layer of metal or dielectric material using PVD/CVD and photolithography.

The unquestionable advantages of interference filters versus absorption filters are the possibility to obtain the desired band-edge position and width, T% and R%, by only changing the number and thickness of the alternating layers in the case of multilayered stacks, or by the type and spacing and the shape of openings/pillars, in the case of the sub-wavelength structures/grids. With these interference structures, band-edge position over the whole visible-NIR region, band-edge widths as low as 10 nm, R% of 99.99% and T% close to 100% for filters with thickness as low as few micrometers, are reported in the literature.[11]

Sub-wavelength grids are chosen as the favorite interference filter candidates, in order to limit the possible temperature exposition during processing of the optical filter, towards an easier/compatible integration process onto the OPT. Indeed, filters based on stacks of active materials require large numbers of layers in order to reach high attenuation (large R%). On the other hand, the technique based on sub-wavelength grids only requires the deposition of one metal layer, so the temperature exposition of the OPT can be limited to a minimum during integration.

In order to evaluate the feasibility/suitability of the selected technology for the optical filter into the optoplasmonic module, first simulations of sub-wavelength gratings were performed. The simulated structures consist of metallic cylinders (200 nm in diameter) in a 500 nm pitch. Figure 15 shows the used unit cell of the grid and the transmission spectra for aluminum and gold structures replicating this unit cell. For this first simulations, blocking of an excitation at 750nm was chosen, approximating the above reported requirements (working range of LSPR, selected OLED-fluorophore combination).
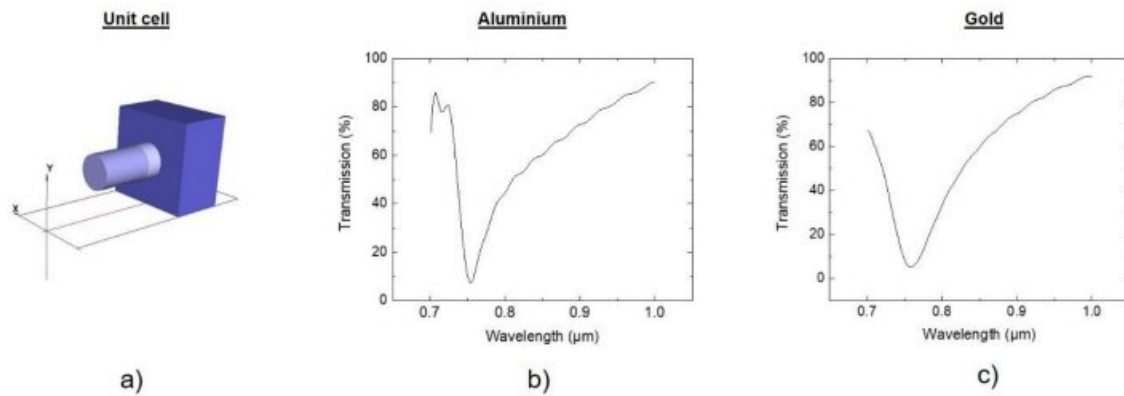
Figure 15. Simulation of sub-wavelength grids: a) unit cell of the grid, b) transmission spectra for aluminum and c) transmission spectra for gold

As a result of the simulation, light at a peak wavelength of 750 nm could be blocked by using the given simple structure. Only a minimum T% of 3% has been achieved during the first simulations, meaning a low rejection ability of the backscattered OLED light. However, as a proof of principle, the selected approach seems promising: improved performance may be obtained by fine tuning the unit cell structure.

Alternatively, larger R% (and lower angular dependency of transmission) could be possibly obtained by combining stacks of sub wavelength structured (Figure 16, taken from ref. 13), which will be possibly also evaluated for integration,in T2.2.
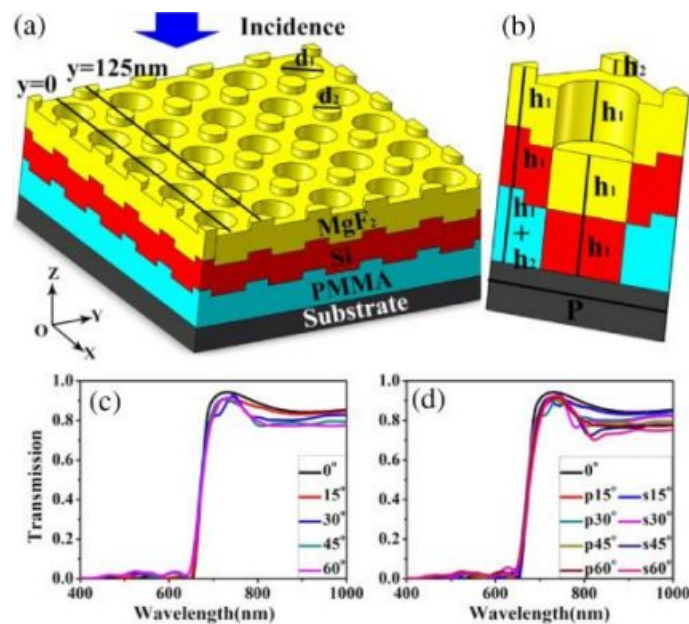
Figure 16. a, b) Stacked sub-wavelength structures. c) and d) transmission spectra for different angels and polarizations [13].

As a final remark, to overcome some further limitations in terms of compatibility of the fabrication processes, a possible bck-up strategy is the use of commercial plastic filters (hundreds of micrometers thick) to be integrated by lamination or gluing onto the OPT. However, any potential issues of this approac, regarding geometrical and optical requirements/constrains on the integrated optoplasmonic mocule, will be accurately taken into account in Task 1.4, System-engineering for a functional prototype.

5   Conclusions

We identified the optical characteristics of the optoplasmonic module components to enable their effective cooperation for LSPR and PEF detection.

<u>OLEDs and OPT</u>

According to the characteristics of the NPG, the preferred spectral region for LSPR is around 770nm. Therefore, the OLED for LSPR will be based on a Pt(tpbp):Alq$_3$ emitter.
According to the characteristics of the NPG and on the final selection of the Fluorophore(s) (please consider D1.2), the most-suitable spectral region for PEF is 520 - 820 nm. Six possible OLEDs for PEF were analyzed in-depth.

Given the spectral regions of interest for LSPR and PEF, the OPT must have a high EQE in the spectral range 520 - 820 nm. The two selected options for the photoactive materials of the OPT are the DPPDTT:PCBM blend, and the ZnPc:C60 blend.

By considering the calculations on the expected efficiency of PEF detection (represented by the PEF factor), in the following best combinations of OLEDs (together with the selected emitter) and Fluorophores are found:

- OLED (Ir(piq)$_3$) – AlexaFluor 750   [PEF factor = 803]
- OLED (Ir(piq)$_3$) – ATTO 700   [PEF factor = 347]
- OLED (Ir(piq)$_3$) – ATTO 740   [PEF factor = 223]
- OLED (Pt(OEP)) – AlexaFluor 750   [PEF factor = 182]
- OLED (Ir(ppy)$_3$) – ATTO 620   [PEF factor = 58.9]

Within these options, we have selected the combination with the highest PEF factor and the combination with the largest spectral separation between the OLED electroluminescence peak wavelength and the Fluorophore fluorescence peak wavelength, in order to facilitate the filter development. Best options, compared to the other, may allow the use of optical filters with larger band-edge width and may allow a larger signal-to-noise ratio.

<u>Selected combination are:</u>

- OLED (Ir(piq)$_3$) – AlexaFluor 750 (highest PEF factor)
- OLED (Pt(OEP)) – AlexaFluor 750 (largest spectral shift)

<u>Optical Filter</u>

According to the best OLED/Fluorophore combinations, and to the OLED selected for LSPR, the optical filter should have a band-edge between 700 and 750 nm. Since the optical filter should be processed onto the OPT with compatible processing conditions, interference filters based on sub-wavelength gratings are proposed as the preferred options. Simulations on such simple structures may lead to a low rejection (3%) in of the OLED excitation region and to a band edge width >100 nm. Such values could be not sufficient, therefore sub-wavelength multilayered stacks (Bragg reflectors) will be also evaluated.

A possible further issue with optical filters (especially in the case of multilayered stack) is that the processing compatibility with OPT could be low, both in the case of solution or vapor/sputtering deposition methods. Back-up strategies include the implementation of i) protecting layers onto the OPT, or ii) integration of laminated/glued thin film commercial filters.

New calculations will be reported in D1.4 and D1.5 quantifying the effects of transmittance, rejection, band-edge width and angular-dependent reflectance of the optical filter, at a selected band-edge, on PEF and LSPR signals. New calculations will also consider: i) the optoplasmonic module layout, ii) the optical power of the OLEDs, iii) the responsivity and EQE of the OPT, iv) the angular response of the NPG. These calculations will lead to an absolute estimation of the expected PEF and LSPR signals.

6 References

1. Giudicatti, S., Marabelli, F. & Pellacani, P. Field Enhancement by Shaping Nanocavities in a Gold Film. *Plasmonics* **8**, 975–981 (2013).

2. Sudheendran Swayamprabha, S. *et al.* Approaches for Long Lifetime Organic Light Emitting Diodes. *Adv. Sci.* **8**, 1–29 (2021).

3. Li, Q., Guo, Y. & Liu, Y. Exploration of Near-Infrared Organic Photodetectors. *Chem. Mater.* **31**, 6359–6379 (2019).

4. Xu, H. *et al.* A high-sensitivity near-infrared phototransistor based on an organic bulk heterojunction. *Nanoscale* **5**, 11850–11855 (2013).

5. Pérez-Rodríguez, A., Temiño, I., Ocal, C., Mas-Torrent, M. & Barrena, E. Decoding the Vertical Phase Separation and Its Impact on C8-BTBT/PS Transistor Properties. *ACS Appl. Mater. Interfaces* **10**, 7296–7303 (2018).

6. Sheraw, C. D., Jackson, T. N., Eaton, D. L. & Anthony, J. E. Functionalized pentacene active layer organic thin-film transistors. *Adv. Mater.* **15**, 2009–2011 (2003).

7. Chaudhry, M. U. *et al.* Nano-Alignment in Semiconducting Polymer Films: A Path to Achieve High Current Density and Brightness in Organic Light Emitting Transistors. *ACS Photonics* **5**, 2137–2144 (2018).

8. Walker, D. E. *et al.* High mobility indium zinc oxide thin film field-effect transistors by semiconductor layer engineering. *ACS Appl. Mater. Interfaces* **4**, 6835–6841 (2012).

9. Wei, S. *et al.* Flexible Quasi-2D Perovskite/IGZO Phototransistors for Ultrasensitive and Broadband Photodetection. *Adv. Mater.* **32**, 1–9 (2020).

10. Bharadwaj, P. & Novotny, L. Spectral dependence of single molecule fluorescence enhancement. *Opt. Express* **15**, 14266 (2007).

11. Dandin, M., Abshire, P. & Smela, E. Optical filtering technologies for integrated fluorescence sensors. *Lab Chip* **7**, 955–977 (2007).

12. Yamazaki, M., Krishnadasan, S., Demello, A. J. & Demello, J. C. Non-emissive plastic colour filters for fluorescence detection. *Lab Chip* **12**, 4313–4320 (2012).

13. Qian, Q., Fan, L., Zhao, L. & Wang, C. Non-metallic and angular-insensitive metasurface transmissive long-pass filter in the visible and near-infrared regions. *Opt. Lett.* **45**, 359 (2020).